



Degradation of Surface Passivation and Bulk in p-type Monocrystalline Silicon Wafers at Elevated Temperature

Kyung Kim , Ran Chen, Daniel Chen , Phillip Hamer, Alison Ciesla nee Wenham, Stuart Wenham, and Ziv Hameiri

Abstract—The surface passivation quality and the bulk lifetime of boron-doped p-type Czochralski silicon wafers were studied in response to dark annealing at 175 °C, using *in situ* effective lifetime measurements. We investigated non-fired and fired silicon nitride (SiN_x), aluminum oxide (AlO_x) capped with SiN_x , and thermally-grown silicon oxide (SiO_2). Modulation in surface passivation quality and bulk lifetime was detected only in cases where hydrogen is assumed to be released into the silicon wafer from the dielectric ($\text{AlO}_x/\text{SiN}_x$ stack and fired SiN_x layer). Interestingly, the degradation of both the surface and the bulk were followed by a recovery. It is also interesting to note that the changes in the surface and the bulk seem to be related, as the surface degradation starts when the initial bulk degradation ends. This study indicates a possible involvement of hydrogen in both the degradation and the recovery processes. The evolution of the effective lifetime as a function of time is similar to that reported for carrier-induced degradation in multicrystalline wafers; however, occurring on a different time scale. Hence, these findings may also be valuable for investigation of other degradation mechanisms in different silicon materials.

Index Terms—Aluminum oxide, crystalline silicon, degradation, hydrogen, silicon nitride, surface passivation.

I. INTRODUCTION

IMPROVING the reliability of photovoltaic (PV) systems is a key requirement for making PV energy cheaper. A recent report by the US Department of Energy indicates that reducing the degradation of PV systems is a very promising method of lowering the price of PV energy [1], especially considering that increasing the efficiency is becoming more difficult as the fundamental limit is approached.

Manuscript received March 30, 2018; revised August 2, 2018 and September 15, 2018; accepted October 24, 2018. This work was supported in part by the Australian Government through the Australian Renewable Energy Agency under Project 2017/RND001, and in part by the Australian Research Council under Project DE150100268. (Corresponding author: Kyung Kim.)

K. Kim, R. Chen, D. Chen, A. Ciesla nee Wenham, and Z. Hameiri are with the University of New South Wales, Sydney, NSW 2052, Australia (e-mail: k.h.kim@student.unsw.edu.au; ran.chen@unsw.edu.au; daniel.chen@unsw.edu.au; a.ciesla@unsw.edu.au; ziv.hameiri@unsw.edu.au).

P. Hamer is with the University of New South Wales, Sydney, NSW 2052, Australia, and also with the Oxford University, Oxford OX1 3PH, U.K. (e-mail: phil.hamer@materials.ox.ac.uk).

S. Wenham, deceased, was with the, University of New South Wales, Sydney, NSW 2052, Australia (e-mail: s.wenham@unsw.edu.au).

Color versions of one or more of the figures in this paper are available online at <http://ieeexplore.ieee.org>.

Digital Object Identifier 10.1109/JPHOTOV.2018.2878791

In the past decades, a number of studies have been done to identify and investigate various degradation mechanisms in silicon (Si) solar cells [2]–[16]. One example is the formation of metastable boron–oxygen (BO) related defects in boron-doped p-type Czochralski (Cz) wafers after exposure to light [3], [9]–[11]. Recently, a similar degradation behavior was identified in multicrystalline silicon (mc-Si) wafers [8], [12]–[14]. This degradation, which is known as either light and elevated temperature induced degradation (LeTID; [4], [5], [15], [16]) or carrier induced degradation (CID; [6]–[8]), was found to significantly decrease the efficiency of passivated emitter and rear cells (PERC) fabricated using mc-Si wafers [14]. More recently, it has been reported that LeTID also occurs in Cz wafers [17], [18]. It was demonstrated that the same defect can be formed by purely thermal degradation and regeneration processes in both Cz and mc-Si wafers; hence, light is not required for LeTID [18]. A few studies have suggested involvement of hydrogen in the degradation and regeneration processes [16], [18]–[25]; however, it seems that more work needs to be done in order to fully understand the role of hydrogen in this degradation.

In this study, we aim to assess the impact of hydrogen on both the Shockley–Read–Hall lifetime (τ_{SRH}) and the surface saturation current density (J_{0s}). For that, we use hydrogen-rich dielectrics and dielectrics that are believed to be hydrogen free. We investigate both as-deposited and fired wafers.

Recently Sperber *et al.* [26]–[28] investigated the stability of the surface passivation under light and elevated temperature in order to differentiate the impact of the process on the surface passivation and the bulk quality. They used the slope-based method [29] with improved parameterization to extract J_{0s} from the injection-dependent effective lifetime τ_{eff} measurements [30]. Degradation of the surface passivation (with various dielectrics) was observed in FZ, Cz, and mc-Si wafers, including in BO-regenerated samples [28].

In this study, unlike the work of Sperber *et al.* [26]–[28], we investigate purely thermal-based degradation and regeneration processes by observing samples during dark annealing (DA) at a wafer's temperature of 175 ± 2 °C. This does not seem to be related to the BO defect, which dissociates in the dark [9]; instead we propose the involvement of hydrogen. *In situ* photoconductance (PC) τ_{eff} measurements at elevated temperatures are used to monitor J_{0s} and τ_{SRH} of fired and non-

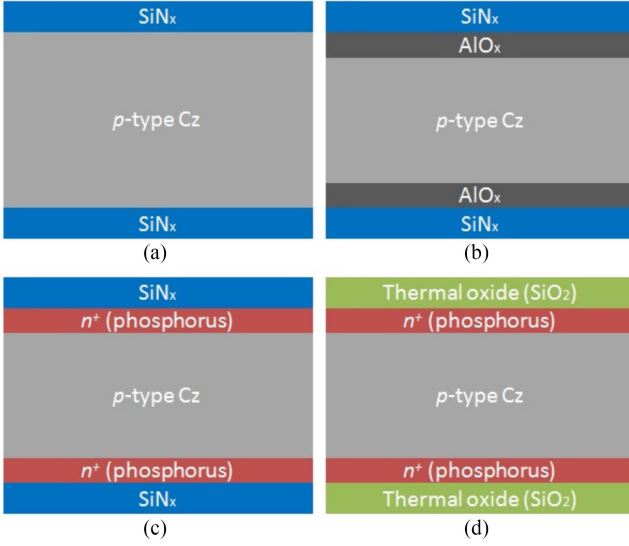


Fig. 1. Four different lifetime test structures. (a) SiN_x . (b) $\text{AlO}_x/\text{SiN}_x$. (c) n^+/SiN_x . (d) n^+/SiO_2 .

fired silicon nitride (SiN_x), aluminum oxide (AlO_x) capped with SiN_x , and thermally-grown silicon oxide (SiO_2) passivated wafers.

II. EXPERIMENT

A. Sample Preparation

Commercially available ($156 \text{ mm} \times 156 \text{ mm}$) boron-doped p-type, Cz wafers, with resistivity of $1.7 \pm 0.2 \Omega \cdot \text{cm}$ (bulk doping concentration of $8.5 \pm 1.2 \times 10^{15} \text{ cm}^{-3}$) and final thickness of $190 \pm 10 \mu\text{m}$, were used in this study. Four different lifetime test structures were fabricated, as shown in Fig. 1.

All the wafers were processed together until the surface passivation stage. They were textured (random upright pyramid) and Radio Corporation of America (RCA) cleaned together [31] before a POCl_3 diffusion to form an electron collector layer (commonly called emitter [32]) with a sheet resistivity of $100 \Omega/\square$ on both sides (process temperatures between 795°C and 885°C [33]). Then, the phosphosilicate glass (PSG) was removed before thermal oxidation at 930°C for 15 min to grow a 50-nm-thick SiO_2 layer [34]. The final sheet resistivity after the oxidation process was $110 \Omega/\square$. For Structure A, B, and C [see Fig. 1(a)–(c)], the oxide was removed using a hydrofluoric acid (HF) solution. A sodium hydroxide solution (mass fraction 30%) was then used to etch the diffused layer ($\sim 1 \mu\text{m}$) from both sides of Structure A–B at a temperature of 85°C .

An industrial in-line plasma-enhanced chemical vapor deposition (PECVD) system (MAiA, Meyer Burger) was used for the deposition of both SiN_x and AlO_x at 400°C . A standard SiN_x anti-reflection coating (75 nm thick with a refractive index of 2.08 at 633 nm) was used for Structure A and C [35], while a 16-nm-thick AlO_x layer with a refractive index of 1.59 was used for Structure B. The AlO_x was then capped with SiN_x deposited at 350°C to minimize possible modification of both the bulk and the existing AlO_x [36].

Each wafer was then laser cleaved into 16 tokens ($39 \text{ mm} \times 39 \text{ mm}$). After cleaving, half of the wafer tokens remained as-deposited (hereafter non-fired), while the other half underwent a fast firing process in an industrial metallization furnace (7K9-70C69-5LIR, Schmid) with clean dry air (CDA) ambient. The set firing temperature was adjusted to maintain a fixed wafer temperature of $740 \pm 5^\circ\text{C}$ for all the wafers, and the duration at the peak temperature was about 0.5 s.

B. Measurement Procedures

Samples were dark annealed at $175 \pm 2^\circ\text{C}$. *In situ* PC lifetime measurements were made using a lifetime tester (WCT-120TS from Sinton Instruments). The samples were kept in the dark for the entire time (during measurements and between measurements). We therefore assume no external influence of BO defects on the obtained results, especially considering the DA temperature [9]. To determine τ_{eff} at elevated temperature, the Dörkel–Leturcq mobility model [37] was used. The surface passivation quality was assessed by extraction of J_{0s} from the Auger-corrected τ_{eff} measurements using the Kane–Swanson method [29] and the intrinsic carrier concentration model that is implemented in the system [38]. Since the Auger lifetime remains almost constant from room temperature up to 200°C [39] and following Sinton Instrument recommendation [40], the Auger model of Richter *et al.* was used in this study [41]. The value of J_{0s} was extracted at an excess minority carrier concentration (Δn) of 10^{16} cm^{-3} using a linear fit in the range between $7 \times 10^{15} \text{ cm}^{-3}$ and $1.3 \times 10^{16} \text{ cm}^{-3}$. The intercept of the linear fit with the y-axis provides an estimation of τ_{SRH} at high injection.

To validate the extracted J_{0s} and τ_{SRH} , Quokka 2 [42] was used to fit representative τ_{eff} measurements (at the end of each stage, see Section III below). From the highly accurate Quokka-based fits ($R^2 > 0.99$), J_{0s} , and τ_{SRH} were extracted without any assumption regarding the uniformity of Δn profile [43] and the injection dependence of τ_{SRH} . Despite the expected slight differences in the absolute values (due to the limitations of the slope-based methods [44]), the two methods are in good agreement regarding the trend of the values, which is the key information for this study. More information regarding the Quokka models can be found in Appendix A.

While recombination at the edges can influence lifetime measurements of small samples [45], [46], Chan *et al.* confirmed that the edge recombination does not have impact on lifetime measurements at high injection ($\Delta n > 10^{15} \text{ cm}^{-3}$) [47]. Since the analysis in this study was carried out at $\Delta n > 7 \times 10^{15} \text{ cm}^{-3}$, we assume the measurements are unaffected by edge recombination. This was also supported by PL images at various intensities, which indicate that the edge-impacted regions extend less than 1 mm from the edges. The PL images also confirm that all samples used are free from scratches that could otherwise impact measurements. Additionally, the sensed area in the WCT-120TS is smaller than the sensed area of the standard WCT-120, which ensures even smaller impact of the edges.

Note that in the following sections, we present τ_{eff} and τ_{SRH} at 175°C ; the values at this temperature are, of course, different from those at room temperature.

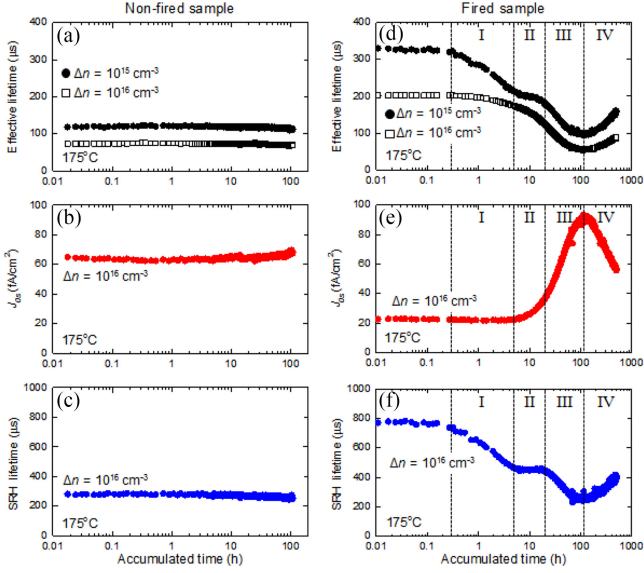


Fig. 2. Evolution of (a) τ_{eff} , (b) J_{0s} , (c) τ_{SRH} for non-fired SiN_x sample, and (d) τ_{eff} , (e) J_{0s} , (f) τ_{SRH} for fired SiN_x sample during DA.

III. RESULTS AND DISCUSSION

A. C-Si/SiN_x Structure

Fig. 2 presents τ_{eff} [(a) and (d); at $\Delta n = 10^{15} \text{ cm}^{-3}$ and $\Delta n = 10^{16} \text{ cm}^{-3}$], the extracted J_{0s} [(b) and (e); at $\Delta n = 10^{16} \text{ cm}^{-3}$], and τ_{SRH} [(c) and (f); at $\Delta n = 10^{16} \text{ cm}^{-3}$] as a function of DA duration. Results for both non-fired and fired SiN_x samples are presented. For the non-fired case [(a)–(c)], there is very little change in the parameters (J_{0s} is degraded by about 5%, τ_{SRH} by about 8%, and τ_{eff} by about 7%) during the entire 110 h of measurement.

The behavior of the fired sample [see Fig. 2(d)–(f)], however, is very different. First, as expected, the firing process improves both the surface passivation quality (J_{0s} decreases from 63 fA/cm^2 to 22 fA/cm^2) and the bulk (τ_{SRH} increases from 280 to 770 μs). This improvement can be attributed to hydrogen release from the SiN_x layer [48], which passivates both dangling bonds at the surface [49], [50] and bulk defects [51], [52]. Interestingly, τ_{SRH} starts to degrade after 0.3 h of DA process. At this stage (Stage I in Fig. 2), no change in J_{0s} is observed. The decrease in τ_{eff} (at $\Delta n = 10^{15} \text{ cm}^{-3}$) can be therefore correlated solely with the degradation of the bulk quality. Stage I lasts for 5 h. After 5 h (Stage II), τ_{SRH} plateaus, while the surface passivation starts to degrade (J_{0s} increases).

In Stage III (between 20 and 110 h), both the surface and the bulk degrade, again resulting in a degradation of τ_{eff} . Note that during Stages I and III, changes in τ_{eff} cannot be interpreted whether the degradation is attributed to the bulk or at the surface, alone. At the most degraded state (at 110 h of DA), the surface quality is lower than the level of the non-fired sample, whereas the bulk quality is about the same. As discussed below, this may be due to the different impact of hydrogen on the surface and the bulk.

Interestingly, significant improvement of both J_{0s} and τ_{SRH} is observed after 110 h (Stage IV). The improvement (or re-

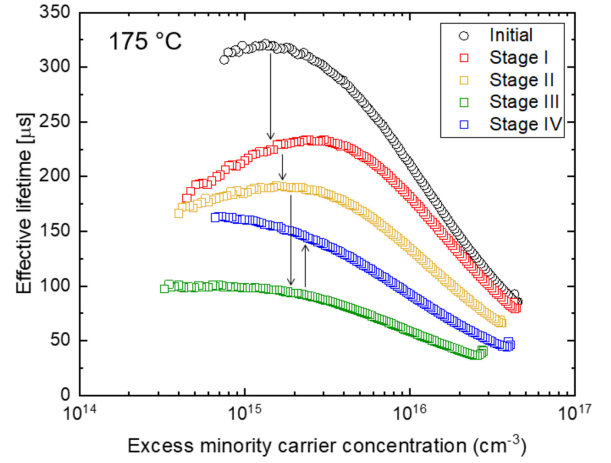


Fig. 3. Injection-dependent effective lifetime curves of a fired SiN_x sample at the end of each stage.

generation) is much slower than the degradation and τ_{eff} does not fully recover to its initial value, even after 500 h. It is also interesting that although the degradation of the surface and the bulk start at different times, their recovery seems to start at the same time. Despite the higher temperature in this study (175 °C in the dark) and the lack of illumination, our observations are similar to the results reported by Sperber *et al.* (150 °C at about 1-sun illumination) [28]. The main difference is that we have not observed an increase in τ_{eff} during Stage II, just a plateau.

Fig. 3 depicts the injection-dependent lifetime of the fired SiN_x wafers. The presented measurements were chosen from the end of each stage. Because it is preferable to extract J_{0s} at high injection [53], measurements were done using high intensity illumination. Hence, the low injection region of τ_{eff} was not collected. This limits our ability to fit the curves in order to extract the defect parameters, particularly for the bulk. It does appear, however, that the τ_{eff} of the degraded sample has only weak injection dependence.

B. C-Si/AlO_x/SiN_x Structure

In this section, we study the stability of samples with an $\text{AlO}_x/\text{SiN}_x$ stack passivation layer. Fig. 4 presents the evolution of τ_{eff} [(a) and (d); at $\Delta n = 10^{15} \text{ cm}^{-3}$ and $\Delta n = 10^{16} \text{ cm}^{-3}$], the extracted J_{0s} [(b) and (e); at $\Delta n = 10^{16} \text{ cm}^{-3}$] and τ_{SRH} [(c) and (f); at $\Delta n = 10^{16} \text{ cm}^{-3}$] as a function of DA duration annealing before and after firing.

We first examine the behavior of the non-fired sample. All the parameters are constant during the first 5 h of DA. After this time, both the surface and the bulk start to degrade at a relatively slow rate. No recovery of these parameters is observed during the 320 h of measurement. A possible reason for the different behavior of this structure, when compared to the non-fired SiN_x sample, could be the release of hydrogen from the AlO_x during the deposition of the SiN_x capping layer. It is possible that some hydrogen may have been released into the bulk during deposition, even without a deliberate firing process. The significantly higher initial τ_{SRH} of the non-fired $\text{AlO}_x/\text{SiN}_x$ sample compared to the non-fired SiN_x sample (580 versus

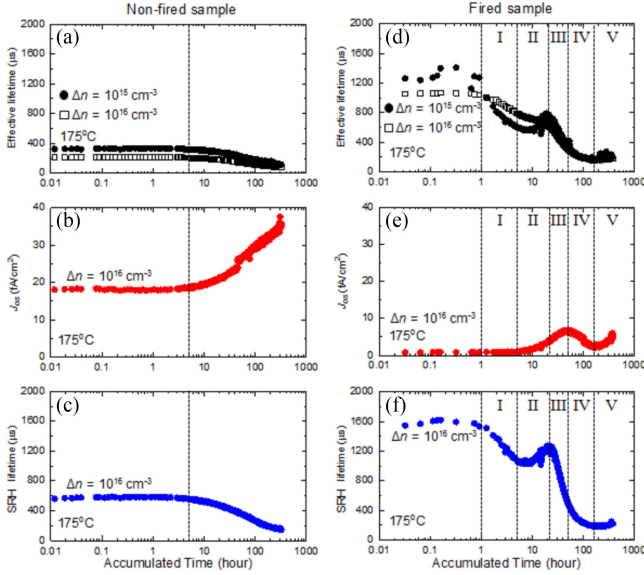


Fig. 4. Evolution of (a) τ_{eff} , (b) J_{0s} , (c) τ_{SRH} for non-fired $\text{AlO}_x/\text{SiN}_x$ sample, and (d) τ_{eff} , (e) J_{0s} , (f) τ_{SRH} for fired $\text{AlO}_x/\text{SiN}_x$ sample during DA.

280 μs) supports this explanation. To confirm the improvement of τ_{SRH} , the non-fired $\text{AlO}_x/\text{SiN}_x$ layer was etched from one of the wafers. The wafer was then cleaned and re-passivated with SiN_x (identical to the one used in Section III-A). The obtained τ_{eff} was found to be higher than that of the wafers directly passivated with the same SiN_x .

To test whether this assumed release of hydrogen during the capping process has any impact on subsequent degradation, we investigated the thermal impact of the SiN_x capping process on a SiN_x sample. We used a non-fired SiN_x sample and mimicked the SiN_x capping layer deposition by passing the sample through the PECVD system but without precursor gases or activation of plasma. Fig. 5 presents the evolution of τ_{eff} , J_{0s} , and τ_{SRH} of the untreated and the thermally treated SiN_x wafers during DA. The τ_{SRH} of the untreated sample degraded by about 8%, whereas the treated sample degraded by about 12%, and a second thermal treatment (not shown) enhanced the degradation even further. With regards to J_{0s} , the untreated sample degraded by about 5%, while the treated sample degraded by about 14%. Hence, it seems that the thermal treatment enhances the degradation of both J_{0s} and τ_{SRH} (and finally of τ_{eff}). It may indicate the possibility that hydrogen is released during the thermal treatment and contributing to the degradation shown in Fig. 5. This increased degradation following the thermal treatment can explain the different degradation between the non-fired SiN_x and $\text{AlO}_x/\text{SiN}_x$ samples, although the significance of the degradation is much stronger in the case of $\text{AlO}_x/\text{SiN}_x$. We believe that AlO_x releases more hydrogen at lower temperature ($<500^\circ\text{C}$) than SiN_x , which requires higher temperature ($>600^\circ\text{C}$) to release a significant amount of hydrogen [54]–[57].

We now examine the fired $\text{AlO}_x/\text{SiN}_x$ sample [see Fig. 4(d)–(f)]. Significant improvement is observed both in the surface passivation quality (J_{0s} is reduced) and the bulk (τ_{SRH} of 1500 μs). Due to the very low J_{0s} , τ_{eff} is primarily impacted by τ_{SRH} .

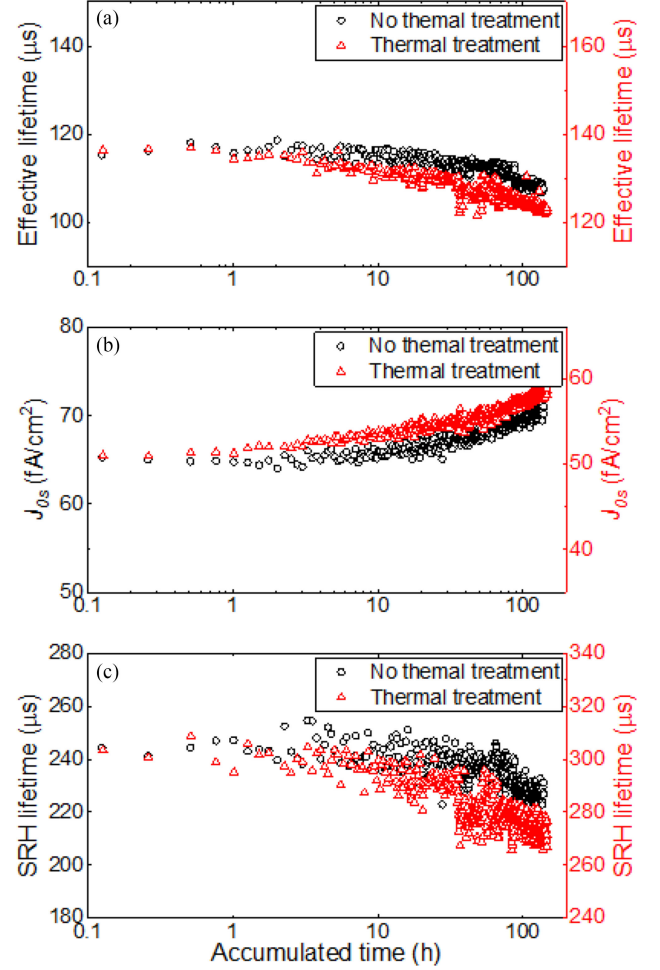


Fig. 5. (a) τ_{eff} , (b) J_{0s} , (c) τ_{SRH} of non-thermally treated and thermally-treated SiN_x samples during DA.

In general, the response of this wafer to the DA is comparable to that of the fired SiN_x sample, however, with a few differences. In Stage I (1–5 h), only the bulk degrades, while J_{0s} seems to be fixed. Note that this stage starts later than the SiN_x case. The surface passivation starts to degrade in Stage II (5–20 h); interestingly, in this case, a bulk improvement is observed (compared to a constant τ_{SRH} in the SiN_x case). However, τ_{SRH} starts to degrade again with continued degradation of the surface in Stage III (20–50 h). After 50 h (Stage IV), J_{0s} starts to decrease (earlier than in the SiN_x case), and recovers almost to its initial value. In contrast with the SiN_x case, no recovery of the bulk is observed during this stage; τ_{SRH} continues to degrade for the rest of the measurement (until 150 h). Stage V is an additional stage that has not been observed for the SiN_x sample. In this stage, the surface passivation degrades again, while τ_{SRH} maintains almost a constant value. These results are similar to those reported about FZ wafers passivated with $\text{AlO}_x/\text{SiN}_x$ [28]. However, in our study, it seems that processes are faster in our study. It may indicate a strong impact of the temperature (175 $^\circ\text{C}$ here, compared to 80 $^\circ\text{C}$ in [28]) on the process and a difference between light (about 1-sun) and temperature. It possibly also indicates a greater hydrogen concentration in our samples.

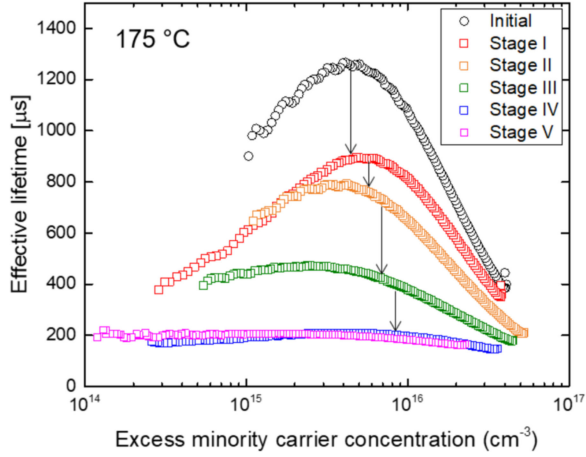


Fig. 6. Injection-dependent effective lifetime curves of a fired $\text{AlO}_x/\text{SiN}_x$ sample at the end of each stage.

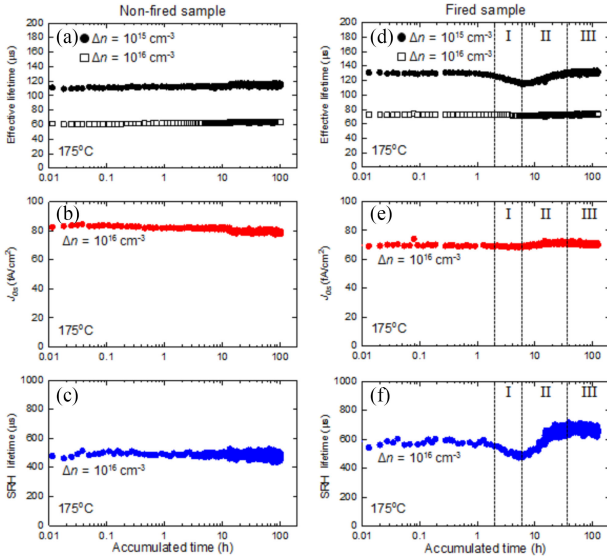


Fig. 7. Evolution of (a) τ_{eff} , (b) J_{0s} , (c) τ_{SRH} for non-fired n^+/SiN_x sample, and (d) τ_{eff} , (e) J_{0s} , (f) τ_{SRH} for fired n^+/SiN_x sample during DA.

Injection-dependent lifetime curves for the fired $\text{AlO}_x/\text{SiN}_x$ sample, at the end of each stage, are shown in Fig. 6. It is observed that the injection level dependence varies for the different stages. It appears that the degraded τ_{eff} has only weak injection dependence, similar to what is observed for the fired SiN_x sample.

C. n^+/SiN_x Structure

To investigate the impact of DA on the front side of a typical solar cell, we now study the n^+/SiN_x structure [see Fig. 1(c)]. With regards to the non-fired diffused sample [see Fig. 7(a)–(c)], the behavior is very similar to the non-diffused sample [see Fig. 2(a)–(c)], where no significant change can be observed in any of the parameters.

No significant improvement was observed in J_{0s} and τ_{SRH} due to firing. The response to DA is quite different for that observed for the SiN_x wafer without the diffused layer [see Fig. 2(d)–(f)].

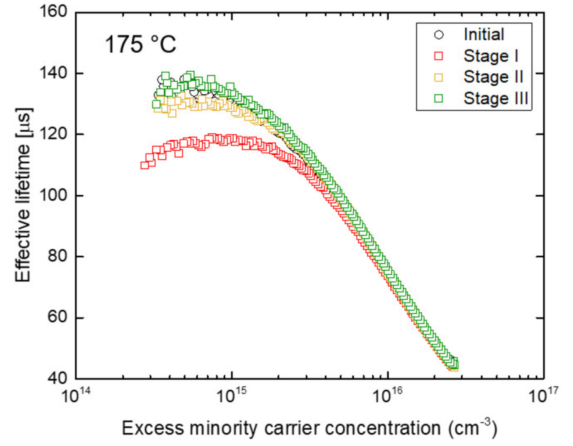


Fig. 8. Injection-dependent effective lifetime curves of a fired n^+/SiN_x sample at the end of each stage.

During Stage I (2–6 h) τ_{SRH} starts to degrade after 2 h of DA and reaches a minimum after 6 h, whereas J_{0s} remains almost constant during this period.

In comparison to the SiN_x sample (see Section III-A), the degradation starts later and the maximum degradation is much less in this case. Between 6 and 36 h (Stage II), τ_{SRH} shows recovery. It is notable that recovery of τ_{SRH} slightly exceeds its initial value by about 12% on average during Stage III (from 36 to 124 h). However, this is not reflected in τ_{eff} as it is dominated by the surface. Note that the behavior of τ_{eff} at 10^{15} cm^{-3} is very similar to that reported for CID in mc-Si [58], however, on a different time scale. This suggests that the degradation and recovery shown here using Cz may have the same root cause as that reported by Chen *et al.* [59].

Injection-dependent lifetime curves of the fired n^+/SiN_x sample at the end of each stage are presented in Fig. 8. Substantial variation is seen in low to medium injection, but there is nearly no change at high injection. The lifetime curve at the end of Stage III is almost identical to the initial value.

D. n^+/SiO_2 Structure

Fig. 9 presents results of the thermally grown SiO_2 sample (Structure D in Fig. 1). No significant changes were noted in any of the parameters during the DA process for both fired and non-fired wafers (less than 6%). This is very different from all the other layers studied in this work. Direct comparison can be made between these results and the results presented in the previous section (see Section III-C). The wafers were processed together and have the same diffused n^+ layer; the only difference is the surface passivation layer. Therefore, the different behaviors of the fired wafers [see Fig. 7(d)–(f) and Fig. 9(d)–(f)] may indicate involvement of hydrogen in the degradation and recovery processes. We assume that the hydrogen concentration in the SiO_2 is very low, if not zero. This may also support numerous studies that suggested hydrogen involvement in CID [22], [23], [25], [59], [60]. A correlation (between released hydrogen fraction and the degradation extent) was observed in our recent study of mc-Si wafers [8].

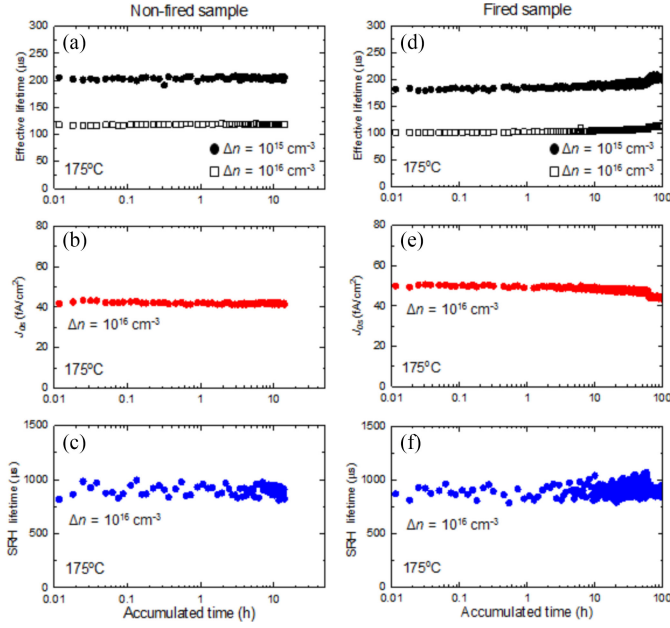


Fig. 9. Evolution of (a) τ_{eff} , (b) J_{0s} , (c) τ_{SRH} for non-fired n^+/SiO_2 sample, and (d) τ_{eff} , (e) J_{0s} , (f) τ_{SRH} for fired n^+/SiO_2 sample during DA.

E. Proposed Hydrogen-Based Model

In this section, we discuss possible root causes of degradation/regeneration and how they may be explained with regard to the behavior of hydrogen in the samples. Our main observations are as follows.

- 1) There is a significant difference between fired and non-fired samples [see Figs. 2, 4, and 7].
- 2) The bulk degrades earlier than the surface for the fired samples [see Figs. 2(d)–(f) and 4(d)–(f)].
- 3) The starting point for surface degradation appears to be very close to the point at which the initial bulk degradation reach saturation [see Fig. 2(d)–(f)] and start to “regenerate” [see Fig. 4(d)–(f)].
- 4) None of the observations above [(1)–(3)] occur in the sample passivated with SiO_2 , which is believed not to contain hydrogen.

We explain Observation (1) and (4) by assuming that the bulk defects formed in Stage I are related to the hydrogen concentration in the Si bulk. This is supported by a range of studies in the literature [5], [8], [58]. Therefore, the initial decay of the bulk lifetime [see Observation (2)] can be explained as the formation of hydrogen-related bulk defects, with a time scale determined by the release rate of hydrogen from recombination *inactive* states (such as hydrogen dimers or similar [61]) throughout the bulk. In the case of non-fired SiN_x , much less hydrogen is released from the dielectric layer, and hence this initial bulk degradation is not observed.

The obvious question then becomes: What is the cause of the subsequent “regeneration” and can it be related to an increase in surface recombination [see Observation (3)]? There are at least three plausible hydrogen-related explanations, but only one of them can be linked to recombination at the surface. The first one

is that as additional hydrogen becomes available, it passivates the hydrogen-related defects and reduces their recombination activity. There is significant evidence for this in the interaction of hydrogen with several interstitial metals [62]–[67]. The second explanation is that over time hydrogen de-bonds from the hydrogen-related defect and forms more stable, recombination-inactive forms. The third explanation is a special case of the second explanation in which the hydrogen de-bonds from the defects and migrates from the Si bulk toward the surface. This has been simulated at elevated temperatures in the presence of an emitter [57]; however, the results of Bredemeier *et al.* [68] support the view that it is also possible where no emitter is present. This process is a more likely explanation of our results. In order to account for the results presented in this study, the migration of hydrogen to the surface must have different effects for different passivation layers and doping profiles. In the case of non-fired SiN_x , the surface degradation is significantly less; as again, much less hydrogen is released from the dielectric layer in that case.

In the case of a SiN_x passivated surface on p-type Si we would expect the presence of an inversion layer at the surface [49], [69], [70]. Examining the changes in Fig. 2(e) and (f) during Stages III and IV indicates that the changes in J_{0s} and τ_{SRH} are almost exactly correlated. This could be a result of the formation and subsequent dissolution of hydrogen-related defects within the inversion layer as previously observed and modeled by Steingrube *et al.* [71]. However, if the hydrogen that forms these defects comes from the Si bulk rather than the surface, an alternate defect distribution (and hence different injection level dependence) is expected. If this is the case, it means that the second bulk lifetime decrease seen in Fig. 2(f) is likely an artifact caused by using the Kane–Swanson method on a structure with an injection-level-dependent J_{0s} term.

In contrast, the surface of a p-type wafer passivated by a fired $\text{AlO}_x/\text{SiN}_x$ stack is expected to be in accumulation [72], [73]. Not only is the formation of hydrogen-related defects likely to be different under these conditions, but the effect of these defects (if present) on the total effective lifetime will be reduced. This is in reasonable agreement with the modest changes in J_{0s} observed in Fig. 4(e). It should also be noted that the electric field in the accumulation condition due to negative fixed charge in AlO_x layer will drive H^+ , the dominant form of interstitial hydrogen in p-type Si [74], [75], further toward the surface and may result in more significant effusion of hydrogen from the Si surface.

In the case where the surface is heavily doped [see Fig. 7(d)–(f)], hydrogen migrating to this region will likely be trapped in the heavily phosphorus-doped region [57]. Given the high availability of ionized dopant ions that act as effective traps for hydrogen [76], the formation of hydrogen-related defects is likely suppressed; hence, no notable change in J_{0s} is observed.

Although this model explains most of the results, it still leaves two effects unexplained. The first is the two-stage degradation in bulk lifetime observed in fired sample passivated with $\text{AlO}_x/\text{SiN}_x$ [see Fig. 4(f)]. The second is the correlated increase in surface and bulk degradation observed in unfired sample passivated with $\text{AlO}_x/\text{SiN}_x$ [see Fig. 4(b) and (c)].

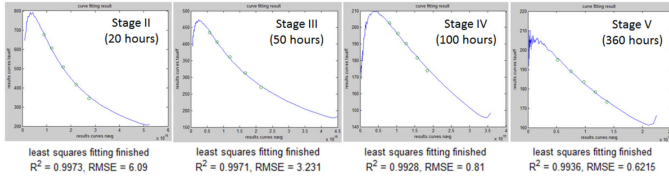


Fig. 10. Quokka 2 modeling results for each stage of the fired $\text{AlO}_x/\text{SiN}_x$ sample.

At this stage, our best explanation for the second degradation in bulk lifetime is dissociation of hydrogen from previously passivated bulk defects. If effusion of hydrogen from the p-type bulk is indeed enhanced by the presence of an accumulation region, as compared to an inversion region, it is possible that the bulk of the wafer becomes so denuded that previously passivated defects cannot be re-passivated once hydrogen has dissociated from them. While this explanation requires much more rigorous investigation, there is some support in the observation that the lifetime decays to a similar level of the non-fired SiN_x sample that are presumed to contain minimal hydrogen. It is also possible that a second source of hydrogen with a different activation energy for slower release exists in the bulk that causes the second degradation as reported in the previous studies [77], [78].

The behavior of the non-fired $\text{AlO}_x/\text{SiN}_x$ sample, which has hydrogen released from the AlO_x layer during the SiN_x deposition is also difficult to explain. Since the hydrogen diffuses into the bulk at temperature about 350°C , there is likely to be a significant concentration gradient from the surface to the bulk. With subsequent annealing at 175°C this hydrogen may diffuse further into the sample forming recombination-active defects as seen in other samples.

IV. CONCLUSION

Stability of surface passivation and Si bulk passivation at elevated temperature in the dark was studied. It was confirmed that different surface passivation layers demonstrate different behaviors in terms of the surface passivation and the Si bulk quality. By investigating the separated components of the surface and the bulk, it was possible to identify that their degradations have different kinetics and severity. For the same surface passivation layer, it is the firing process that activates the degradation. It was also found that even the deposition temperature can activate the degradation.

Changes in J_{0s} and τ_{SRH} were detected only in cases where hydrogen is assumed to be released into the wafer from the dielectric ($\text{AlO}_x/\text{SiN}_x$ stack and fired SiN_x layer). No degradation has been observed in wafers passivated by thermally grown SiO_2 , which is assumed to contain no hydrogen. It was also shown that the presence of a heavily doped n^+ region has significant impact on the modulation of both surface and bulk passivation.

The results were explained based on possible involvement of hydrogen in both the degradation and the recovery processes. Further investigation is required to enable greater certainty

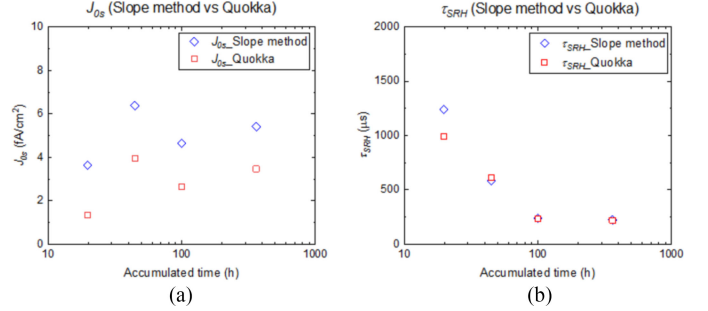


Fig. 11. Comparison between the values extracted by slope method and Quokka fitting for (a) J_{0s} and (b) τ_{SRH} .

around this explanation and its implications for other types of degradation in crystalline Si solar cells.

APPENDIX

The advanced physical models in Quokka 2 [42] were used to fit the lifetime measurements. We tested two approaches: (1) fitting using an injection-dependent τ_{SRH} and a constant J_{0s} , and (2) fitting using a constant τ_{SRH} (at high injection) and a constant J_{0s} . Since our measurements were performed at high injection, we have not observed any advantage of using injection-dependent τ_{SRH} : The fit quality and the extracted values were similar to the second approach. We, therefore, used constant τ_{SRH} (at high injection) and a constant J_{0s} for the fit. To investigate the uniqueness of the fit and the associated uncertainty, we fixed J_{0s} at 10% and 20% lower and higher values than the optimum value and re-fitted τ_{SRH} . We have noticed that 10% variation in J_{0s} is sufficient to reduce the quality of the fit, indicating that the extracted values form unique parameter pairs. J_{0s} and τ_{SRH} were extracted from the excellent fits ($R^2 > 0.99$) at the end of each stage for all the cases. Fig. 10 presents representative Quokka-based fits, while Fig. 11 shows a comparison between values obtained by the two methods. Although the slope-based method results in higher J_{0s} values, the obtained trends by the two methods agree very well, which is the key information of this study. Similar results are obtained for τ_{SRH} .

REFERENCES

- [1] J.-A. Becca, "Sunshot 2030," in *Proc. 44th IEEE Photovolt. Specialist Conf.*, 2017, pp. 15–20.
- [2] J. Lindroos and H. Savin, "Review of light-induced degradation in crystalline silicon solar cells," *Sol. Energy Mater. Sol. Cells*, vol. 147, pp. 115–126, 2016.
- [3] S. W. Glunz, S. Rein, W. Warta, J. Knobloch, and W. Wettling, "Degradation of carrier lifetime in Cz silicon solar cells," *Sol. Energy Mater. Sol. Cells*, vol. 65, no. 1, pp. 219–229, 2001.
- [4] A. E. Morishige *et al.*, "Lifetime spectroscopy investigation of light-induced degradation in p-type multicrystalline silicon PERC," *IEEE J. Photovolt.*, vol. 6, no. 6, pp. 1466–1472, Nov. 2016.
- [5] M. A. Jensen, A. E. Morishige, J. Hofstetter, D. B. Needleman, and T. Buonassisi, "Evolution of p-type LeTID defects in multicrystalline silicon during degradation and regeneration," *IEEE J. Photovolt.*, vol. 7, no. 4, pp. 980–987, Jul. 2017.
- [6] C. E. Chan *et al.*, "Rapid stabilization of high-performance multicrystalline p-type silicon PERC cells," *IEEE J. Photovolt.*, vol. 6, no. 6, pp. 1473–1479, Nov. 2016.

- [7] D. N. R. Payne *et al.*, "Rapid passivation of carrier-induced defects in p-type multi-crystalline silicon," *Sol. Energy Mater. Sol. Cells*, vol. 158, no. Part 1, pp. 102–106, 2016.
- [8] C. Vargas *et al.*, "Carrier-induced degradation in multicrystalline silicon: Dependence on the silicon nitride passivation layer and hydrogen released during firing," *IEEE J. Photovolt.*, vol. 8, no. 2, pp. 413–420, 2018.
- [9] K. Bothe and J. Schmidt, "Electronically activated boron-oxygen-related recombination centers in crystalline silicon," *J. Appl. Phys.*, vol. 99, no. 1, pp. 013701-1-013701-11, 2006.
- [10] T. Niewelt, J. Sch. W. Warta, S. W. Glunz, and M. C. Schubert, "Degradation of crystalline silicon due to boron-oxygen defects," *IEEE J. Photovolt.*, vol. 7, no. 1, pp. 383–398, Jan. 2017.
- [11] B. Hallam *et al.*, "Eliminating light-induced degradation in commercial p-type Czochralski silicon solar cells," *Appl. Sci.*, vol. 8, no. 10, pp. 1–19, 2017.
- [12] K. Ramspeck *et al.*, "Light induced degradation of rear passivated mc-Si solar cells," in *Proc. 27th Eur. Photovolt. Solar Energy Conf. Exhib.*, 2012, pp. 861–865.
- [13] K. Krauss, F. Fertig, D. Menzel, and S. Rein, "Light-induced degradation of silicon solar cells with aluminium oxide passivated rear side," *Energy Procedia*, vol. 77, pp. 599–606, 2015.
- [14] K. Petter *et al.*, "Dependence of LeTID on brick height for different wafer suppliers with several resistivities and dopants," in *Proc. 9th Int. Work. Cryst. Silicon Sol. Cells*, 2016, vol. 6, pp. 1–17.
- [15] F. Kersten *et al.*, "Degradation of multicrystalline silicon solar cells and modules after illumination at elevated temperature," *Sol. Energy Mater. Sol. Cells*, vol. 142, pp. 83–86, 2015.
- [16] K. Nakayashiki *et al.*, "Engineering solutions and root-cause analysis for light-induced degradation in p-type multicrystalline silicon PERC modules," *IEEE J. Photovolt.*, vol. 6, no. 4, pp. 860–868, Jul. 2016.
- [17] F. Fertig *et al.*, "Mass production of p-type Cz silicon solar cells approaching average stable conversion efficiencies of 22%," *Energy Procedia*, vol. 124, pp. 338–345, 2017.
- [18] D. Chen *et al.*, "Evidence of an identical firing-activated carrier-induced defect in monocrystalline and multicrystalline silicon," *Sol. Energy Mater. Sol. Cells*, vol. 172, pp. 293–300, 2017.
- [19] D. Bredemeier, D. Walter, S. Herlufsen, and J. Schmidt, "Lifetime degradation and regeneration in multicrystalline silicon under illumination at elevated temperature," *AIP Adv.*, vol. 6, no. 3, 2016, Art. no. 035119.
- [20] R. Eberle, W. Kwapiel, F. Schindler, M. C. Schubert, and S. W. Glunz, "Impact of the firing temperature profile on light induced degradation of multicrystalline silicon," *Phys. Status Solidi – Rapid Res. Lett.*, vol. 10, no. 12, pp. 861–865, 2016.
- [21] D. Sperber, A. Herguth, and G. Hahn, "Investigating possible causes of light induced degradation in boron-doped float-zone silicon," in *Proc. 33rd EUPVSEC*, 2017, pp. 565–568.
- [22] D. Sperber, A. Herguth, and G. Hahn, "A 3-state defect model for light-induced degradation in boron-doped float-zone silicon," *Phys. Status Solidi – Rapid Res. Lett.*, vol. 11, no. 3, 2017, Art. no. 201600408.
- [23] F. Kersten, J. Heitmann, and J. W. Muller, "Influence of Al₂O₃ and SiN_x passivation layers on LeTID," *Energy Procedia*, vol. 92, pp. 828–832, 2016.
- [24] S. Wilking, A. Herguth, and G. Hahn, "Influence of hydrogen on the regeneration of boron-oxygen related defects in crystalline silicon," *J. Appl. Phys.*, vol. 113, no. 19, 2013.
- [25] N. Nampalli, B. Hallam, C. Chan, M. Abbott, and S. Wenham, "Evidence for the role of hydrogen in the stabilization of minority carrier lifetime in boron-doped Czochralski silicon," *Appl. Phys. Lett.*, vol. 106, 2015, Art. no. 173501.
- [26] D. Sperber, A. Herguth, and G. Hahn, "Instability of dielectric surface passivation quality at elevated temperature and illumination," *Energy Procedia*, vol. 92, pp. 211–217, 2016.
- [27] D. Sperber, F. Furtwangler, A. Herguth, and G. Hahn, "On the stability of dielectric passivation layers under illumination and temperature treatment," in *Proc. 32nd Eur. Photovolt. Solar Energy Conf. Exhib.*, 2016, pp. 523–526.
- [28] D. Sperber, A. Graf, D. Skorka, A. Herguth, and G. Hahn, "Degradation of surface passivation on crystalline silicon and its impact on light-induced degradation experiments," *IEEE J. Photovolt.*, vol. 7, no. 6, pp. 1627–1634, Nov. 2017.
- [29] D. E. Kane and R. M. Swanson, "Measurement of the emitter saturation current by a contactless photoconductivity decay method," in *Proc. 18th IEEE Photovolt. Specialists Conf.*, 1985, pp. 578–583.
- [30] A. Kimmerle, J. Greulich, and A. Wolf, "Carrier-diffusion corrected J₀-analysis of charge carrier lifetime measurements for increased consistency," *Sol. Energy Mater. Sol. Cells*, vol. 142, pp. 116–122, 2015.
- [31] W. Kern and J. E. Soc, "The evolution of silicon wafer cleaning technology," *J. Electrochem. Soc.*, vol. 137, no. 6, pp. 1887–1892, 1990.
- [32] A. Cuevas and D. Yan, "Misconceptions and misnomers in solar cells," *IEEE J. Photovolt.*, vol. 3, no. 2, pp. 916–923, Apr. 2013.
- [33] H. Li, B. Hallam, S. Wenham, and M. Abbott, "Oxidation drive-in to improve industrial emitter performance by POCl₃ diffusion," *IEEE J. Photovolt.*, vol. 7, no. 1, pp. 144–152, Jan. 2017.
- [34] H. Li *et al.*, "POCl₃ diffusion for industrial Si solar cell emitter formation," *Front. Energy*, vol. 11, no. 1, pp. 42–51, 2017.
- [35] Z. Hameiri *et al.*, "Low-absorbing and thermally stable industrial silicon nitride films with very low surface recombination," *IEEE J. Photovolt.*, vol. 7, no. 4, pp. 996–1003, Jul. 2017.
- [36] K. Kim, Z. Hameiri, N. Borojevic, S. Duttagupta, and S. Winderbaum, "Outstanding as-deposited surface passivation by industrial PECVD aluminum oxide," in *Proc. 43rd IEEE Photovolt. Specialists Conf.*, 2016, pp. 2917–2921.
- [37] J. M. Dorkel and P. Leturcq, "Carrier mobilities in silicon semi-empirically related to temperature, doping and injection level," *Solid State Electron.*, vol. 24, no. 9, pp. 821–825, 1981.
- [38] A. B. Sproul and M. A. Green, "Improved value for the silicon from 275 to 375 K intrinsic carrier concentration," *J. Appl. Phys.*, vol. 70, no. 2, pp. 846–854, 1991.
- [39] S. Wang and D. MacDonald, "Temperature dependence of Auger recombination in highly injected crystalline silicon," *J. Appl. Phys.*, vol. 112, no. 11, pp. 3–7, 2012.
- [40] R. A. Sinton, private communication, Mar., 2016.
- [41] A. Richter, F. Werner, A. Cuevas, J. Schmidt, and S. W. Glunz, "Improved parameterization of Auger recombination in silicon," *Energy Procedia*, vol. 27, pp. 88–94, 2012.
- [42] A. Fell, "A free and fast three-dimensional/two-dimensional solar cell simulator featuring conductive boundary and quasi-neutrality approximations," *IEEE Trans. Electron Devices*, vol. 60, no. 2, pp. 733–738, 2013.
- [43] R. Dumbrell, M. K. Juhl, T. Trupke, and Z. Hameiri, "Extracting metal contact recombination parameters from effective lifetime data," *IEEE J. Photovolt.*, vol. 8, no. 6, pp. 1413–1420, Nov. 2018.
- [44] B. Min, A. Dastgheib-Shirazi, P. P. Altermatt, and H. Kurz, "Accurate determination of the emitter saturation current density for industrial p-diffused emitters," in *Proc. 29th Eur. Photovolt. Solar Energy Conf. Exhib.*, 2014, pp. 463–466.
- [45] M. Kessler, T. Ohrdes, P. P. Altermatt, and R. Brendel, "The effect of sample edge recombination on the averaged injection-dependent carrier lifetime in silicon," *J. Appl. Phys.*, vol. 111, no. 5, 2012, Art. no. 054508.
- [46] B. Veith *et al.*, "Injection dependence of the effective lifetime of n-type Si passivated by Al₂O₃: An edge effect?" *Sol. Energy Mater. Sol. Cells*, vol. 120, no. Part A, pp. 436–440, 2014.
- [47] C. E. Chan *et al.*, "Assessing the performance of surface passivation using low-intensity photoluminescence characterization techniques," *IEEE J. Photovolt.*, vol. 4, no. 1, pp. 100–106, Jan. 2014.
- [48] K. Kimura, "Recent developments in polycrystalline silicon solar cells," in *Proc. 1st Int. Photovolt. Sci. Eng. Conf. Tech. Dig.*, 1984, vol. 3741, pp. 37–42.
- [49] A. Cuevas, M. J. Kerr, and J. Schmidt, "Passivation of crystalline silicon using silicon nitride," in *Proc. 3rd World Conf. Photovolt. Energy Convers.*, 2003, pp. 913–918.
- [50] A. G. Aberle, "Surface passivation of crystalline silicon solar cells: a review," *Prog. Photovolt. Res. Appl.*, vol. 8, no. 5, pp. 473–487, 2000.
- [51] R. Hezel and R. Schörner, "Plasma Si nitride - A promising dielectric to achieve high-quality silicon MIS/IL solar cells," *J. Appl. Phys.*, vol. 52, no. 4, pp. 3076–3079, 1981.
- [52] R. Hezel, K. Jaeger, H. L. Tsai, W. F. Richardson, and R. H. Womack, "Low-temperature surface passivation of silicon for solar cells," *J. Electrochem. Soc.*, vol. 136, no. 2, pp. 518–523, 1989.
- [53] H. Mäkel and K. Varner, "On the determination of the emitter saturation current density from lifetime measurements of silicon devices," *Prog. Photovolt. Res. Appl.*, vol. 21, pp. 850–866, 2013.
- [54] G. Dingemans, F. Einsele, W. Beyer, M. C. M. Van de Sanden, and W. M. M. Kessels, "Influence of annealing and Al₂O₃ properties on the hydrogen-induced passivation of the Si/SiO₂ interface," *J. Appl. Phys.*, vol. 111, no. 9, 2012, Art. no. 93713.
- [55] J. K. Holt *et al.*, "Hot-wire chemical vapor deposition of high hydrogen content silicon nitride for solar cell passivation and anti-reflection coating applications," *Thin Solid Films*, vol. 430, no. 1–2, pp. 37–40, 2003.
- [56] F. Jiang *et al.*, "Hydrogenation of Si from SiN_x(H) films: Characterization of H introduced into the Si," *Appl. Phys. Lett.*, vol. 83, no. 5, pp. 931–933, 2003.

- [57] P. Hamer *et al.*, "Modelling of hydrogen transport in silicon solar cell structures under equilibrium conditions," *J. Appl. Phys.*, vol. 123, 2018, Art. no. 043108.
- [58] C. Chan *et al.*, "Modulation of carrier-induced defect kinetics in multicrystalline silicon PERC cells through dark annealing," *Phys. Status Solidi – Rapid Res. Lett.*, vol. 1, 2017, Art. no. 1600028.
- [59] D. Chen *et al.*, "Evidence of an identical firing-activated carrier-induced defect in monocrystalline and multicrystalline silicon," *Sol. Energy Mater. Sol. Cells*, vol. 172, pp. 293–300, 2017.
- [60] S. Wilking, A. Herguth, and G. Hahn, "Influence of hydrogen on the regeneration of boron-oxygen related defects in crystalline silicon," *J. Appl. Phys.*, vol. 113, no. 19, 2013.
- [61] V. V. Voronkov and R. Falster, "Formation, dissociation, and diffusion of various hydrogen dimers in silicon," *Phys. Status Solidi B*, vol. 254, no. 6, 2017, Art. no. 1600779.
- [62] P. M. Williams, G. D. Watkins, S. Uftring, and M. Stavola, "Structure-sensitive spectroscopy of transition-metal-hydrogen complexes in silicon," *Phys. Rev. Lett.*, vol. 70, no. 24, pp. 3816–3819, 1993.
- [63] J.-U. Sachse, E. Ö. Sveinbjörnsson, W. Jost, and J. Weber, "Electrical properties of platinum-hydrogen complexes in silicon," *Phys. Rev. B*, vol. 55, no. 24, pp. 16176–16185, 1997.
- [64] J.-U. Sachse, E. Ö. Sveinbjörnsson, N. Yarykin, and J. Weber, "Similarities in the electrical properties of transition metal-hydrogen complexes in silicon," *Mater. Sci. Eng. B Solid-State Mater. Adv. Technol.*, vol. 58, no. 1, pp. 134–140, 1999.
- [65] S. Knack and J. Weber, "Copper-hydrogen complexes in silicon," *Phys. Rev. B*, vol. 65, 2002, Art. no. 165203.
- [66] N. Yarykin and A. Samples, "Deep levels of copper-hydrogen complexes in silicon," *Phys. Rev. B*, vol. 88, 2013, Art. no. 085205.
- [67] L. Scheffler *et al.*, "Electrical levels in nickel doped silicon," *J. Appl. Phys.*, vol. 116, 2014, Art. no. 173704.
- [68] D. Bredemeier, D. C. Walter, and J. Schmidt, "Possible candidates for impurities in mc-Si wafers responsible for light-induced lifetime degradation and regeneration," *Sol. RRL*, vol. 2, 2018, Art. no. 1700159.
- [69] J. R. Elmiger and M. Kunst, "Investigation of charge carrier injection in silicon nitride/silicon junctions," *Appl. Phys. Lett.*, vol. 69, no. 4, pp. 517–519, 1996.
- [70] G. Beylier, S. Bruyère, D. Benoit, and G. Ghibaudo, "Refined electrical analysis of two charge states transition characteristic of 'borderless' silicon nitride," *Microelectron. Reliab.*, vol. 47, no. 4–5, pp. 743–747, 2007.
- [71] S. Steingrube, P. P. Altermatt, D. S. Steingrube, J. Schmidt, and R. Brendel, "Interpretation of recombination at c-Si/SiN_x interfaces by surface damage," *J. Appl. Phys.*, vol. 108, 2010, Art. no. 014506.
- [72] P. Saint-Cast *et al.*, "Very low surface recombination velocity on p-type c-Si by high-rate plasma-deposited aluminum oxide," *Appl. Phys. Lett.*, vol. 95, no. 15, 2009, Art. no. 151502.
- [73] G. Dingemans and E. Kessels, "Status and prospects of Al₂O₃-based surface passivation schemes for silicon solar cells," *J. Vac. Sci. Technol. A: Vac., Surf. Films*, vol. 30, no. 4, pp. 1–27, 2012.
- [74] S. J. Pearton, J. W. Corbett, and J. T. Borenstein, "Hydrogen in crystalline semiconductors," *Appl. Phys. A*, vol. 43, no. 3, pp. 153–195, 1987.
- [75] C. Herring, N. M. Johnson, and C. G. Van de Walle, "Energy levels of isolated interstitial hydrogen in silicon," *Phys. Rev. B*, vol. 64, no. 12, 2001, Art. no. 125209.
- [76] N. M. Johnson, C. Herring, and D. J. Chadi, "Interstitial hydrogen and neutralization of shallow-donor impurities in single-crystal silicon," *Phys. Rev. Lett.*, vol. 56, no. 7, pp. 769–772, 1986.
- [77] D. Bredemeier, D. Walter, and J. Schmidt, "Light-induced lifetime degradation in high-performance multicrystalline silicon: Detailed kinetics of the defect activation," *Sol. Energy Mater. Sol. Cells*, vol. 173, no. Jul., pp. 2–5, 2017.
- [78] A. Ciesla *et al.*, "Hydrogen-induced degradation," in *Proc. 7th World Conf. Photovolt. Energy Convers.*, 2018.

Authors' photographs and biographies not available at the time of publication.